Comparison of calculated, measured, and beam sampled impedances of a higher-order-mode-damped rf cavity

R. A. Rimmer,[1,*] J. M. Byrd,[1,2] and D. Li[1]

[1]*Lawrence Berkeley National Laboratory, Berkeley, California 94720*
[2]*Department of Physics, University of California, Davis, Davis, California 95616*
(Received 18 February 2000; published 17 October 2000)

Accelerating structures with damped higher-order modes (HOMs) have been the focus of many studies over the past decade. This report compares the results of numerical simulations of damping of HOMs using a new calculation technique applied to the case of the PEP-II rf cavity. We compare these results using this technique, which was not yet developed at the time of the original design, with bench and beam-based measurements of the HOM damping. These results show agreement with bench measurements of the shunt impedances of the strongest HOMs as well as measurements of the beam-induced signals on cavities installed in PEP-II.

I. INTRODUCTION

An rf cavity free of higher-order modes (HOMs) has long been a desire of accelerator builders. The PEP-II rf cavity is from a recent generation of cavity designs with strong damping of the HOMs now in operation [1,2]. The PEP-II design has already proved to be successful in the reduction of coupled-bunch instability growth rates, contributing to the rapid commissioning of the low and high energy rings and the storage of high beam currents, resulting in good luminosity performance. Some of the fabrication principles developed for this project have already been applied to other cavity designs such as the Advanced Light Source third harmonic cavity [3], and the design may provide a basis for cavity designs for future projects such as light sources, storage ring based colliders, and linear collider damping rings [4]. Indeed a scaled version of the PEP-II design was used as the baseline model for the Next Linear Collider damping rings [5,6].

At the time of the original PEP-II cavity design, the techniques available for computing the quality factors (Q's) of HOMs in highly damped structures required large computing times, essentially limiting the analysis to only a few HOMs. Full characterization of the HOMs required construction of a cold-test model of the cavity. Today, the availability of better design tools and faster computers has allowed the development of new techniques for studying the HOM damping. This paper has two main objectives. The first is to describe a time domain simulation technique for computing the HOM damping of highly damped structures using the PEP-II cavity as a model. The second is to compare the simulated performance of the PEP-II cavity using this technique with the measured performance in the laboratory and installed in PEP-II with beam. Section II describes the simulation technique and the results for the PEP-II cavity. Section III describes the laboratory measurements and compares them with the results of Section II. We compare these results with beam-based measurements in Section IV. Conclusions are given in Section V.

II. CALCULATION OF RF PROPERTIES AND HOMS

One of the most difficult tasks in designing a strongly HOM-damped rf cavity is to ensure that all harmful monopole and dipole modes are adequately damped while keeping the efficiency of the accelerating mode as high as possible. The damping scheme developed for the PEP-II cavity uses three waveguides on the cavity body [7], equally spaced around the azimuth, as shown in Fig. 1, so as to couple to all monopole and dipole HOMs. They are positioned so as to couple most strongly to the HOMs with
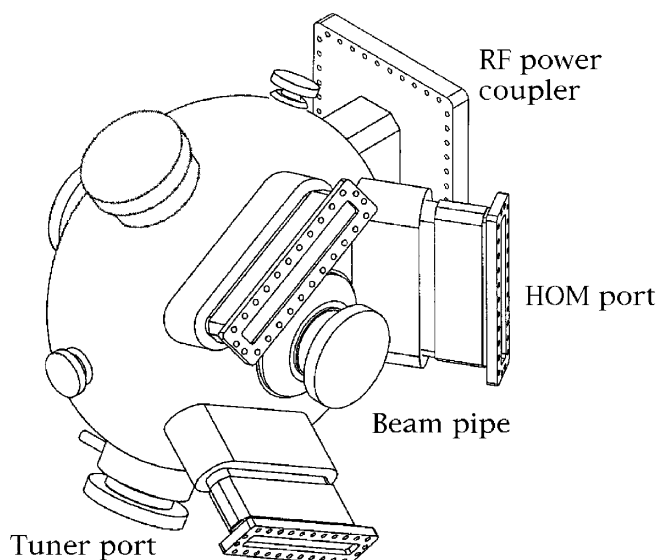

FIG. 1. CAD drawing of the PEP-II cavity. The waveguides are designed to couple to the cavity HOMs.

---

*Corresponding author. Email address: RARimmer@lbl.gov

the highest impedance, particularly the TM_{011} monopole and TM_{110} and TE_{121} dipoles, while not leaving any other harmful modes trapped. The waveguides are wide enough to allow all HOMs to propagate away while retaining the fundamental mode in the cavity. The height of the waveguides is kept small to minimize the loss of cavity surface area in order to keep the Q of the accelerating mode as high as possible.

In the PEP-II cavity design phase the coupling of the waveguide dampers to the cavity HOMs was estimated one mode at a time by a perturbation method [8,9] re-

quiring multiple simulation results per mode, which was time consuming and limited the analysis to only the lower frequency modes. In fact, not all the modes below cut-off could be efficiently calculated using this method. The design was verified for production by extensive measurements of a full-size cold-test model [10], which confirmed the calculated results and showed that the damping scheme was successful for all the harmful modes below cutoff.

With advances in computer speed and new calculation techniques it is now possible to predict the HOM impedance spectrum over a broad frequency range of the
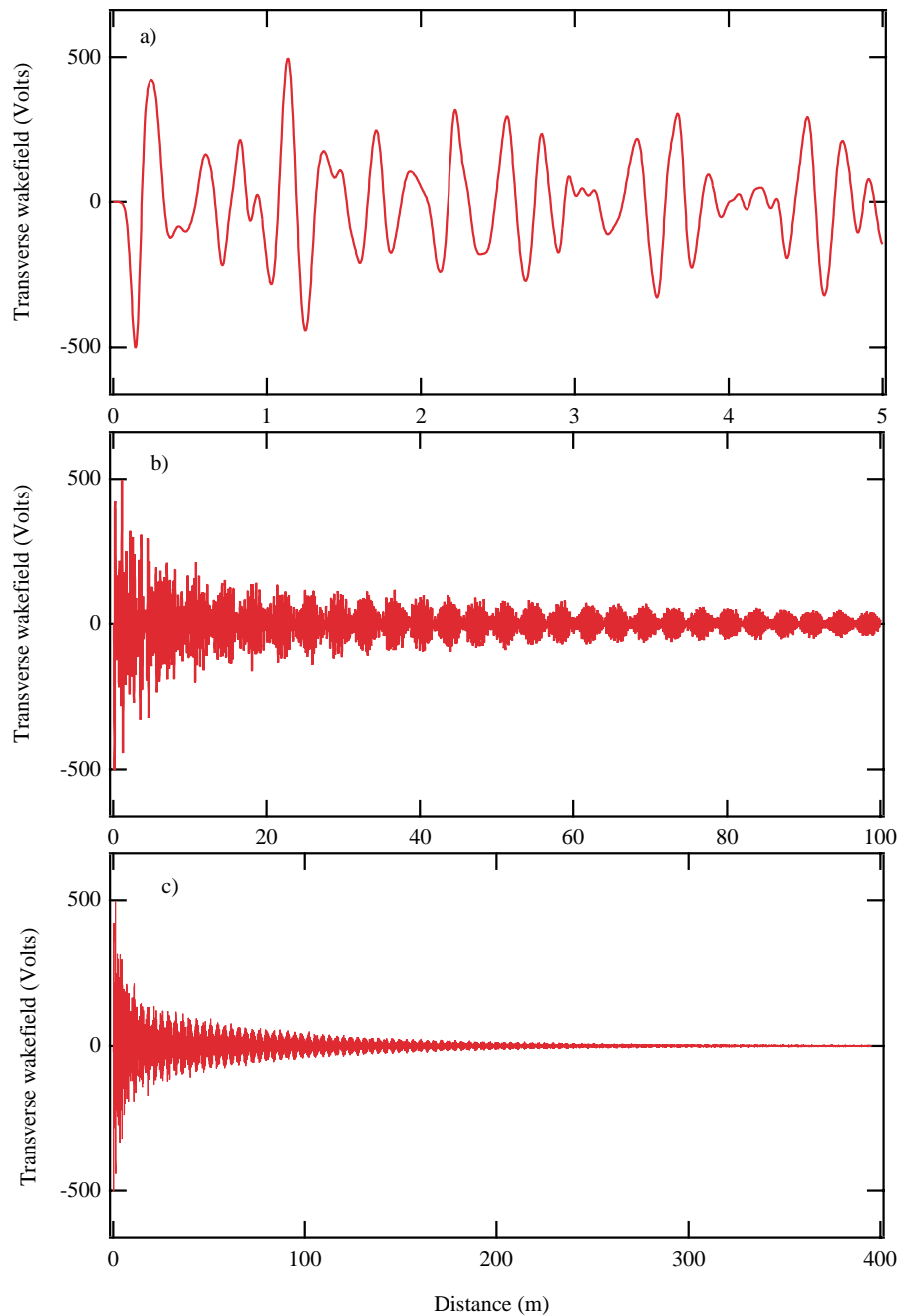

FIG. 2. (Color) Transverse wakefield calculated using MAFIA T3 at 4 cm offset with a 3 cm rms bunch length. (a) Short-range wake, (b) medium-range wake, and (c) long-range wake.

damped cavity in a single run and estimate the strength of all the modes, so long as they do not have very high Q's [11]. This allows the investigation of geometry changes and some degree of optimization to be performed on a reasonable time scale. The method involves a simulation in the time domain using MAFIA in which the structure is excited by a short bunch passing through it, either on axis (for the longitudinal modes) or off axis (for the deflecting modes), and the long range wakefield is computed and recorded for many meters behind the bunch. This time record contains the amplitude of excitation and decay rate of all the excited modes. A Fourier transform of this signal, normalized to the bunch spectrum, gives the impedance spectrum of the cavity. The frequency resolution is determined by the length of the wakefield recorded and the time step interval. In principle, this is limited only by computer time and by the onset of numerical instabilities in the simulation over long time periods. Any mode still ringing with appreciable amplitude at the end of the recorded time will be truncated and artificially broadened in the spectrum, so care must be taken in interpreting the results.

In order to check the validity of these tools the PEP-II cavity geometry was modeled and the results compared with the known cavity properties. Figure 2 shows an ex-

ample of the transverse wake over short, medium, and long time scales. Viewed over a time corresponding to a few periods of the rf frequency, oscillations of individual HOMs are apparent. Over an intermediate time scale, one observes an apparent beating of two residual modes. On the longest time scale, the wake decays completely. The Fourier transform of this wake will give the most accurate model of the impedance spectrum.

Examination of the longitudinal wake in Fig. 3 seems to reveal less because it is dominated by the fundamental mode. Note that the longitudinal wake has not decayed much by the end of the time record. This results in an artificial broadening of the fundamental mode when transformed to the frequency domain. The damping of the wakes of the HOMs is much better studied by transforming the total time domain wake to the frequency domain as discussed below.

The impedance spectra, found from the Fourier transforms of the wakes, provide more insight as shown in Figs. 4(a) and 4(b). Figure 4(a) shows the calculated longitudinal impedance spectrum using this method for the PEP-II geometry, including an approximation of the input power coupler and waveguide. Both the fundamental mode (TM_{010}) and the first monopole HOM (TM_{011}) are marked, as well as the TM beam pipe cutoff frequency, above which
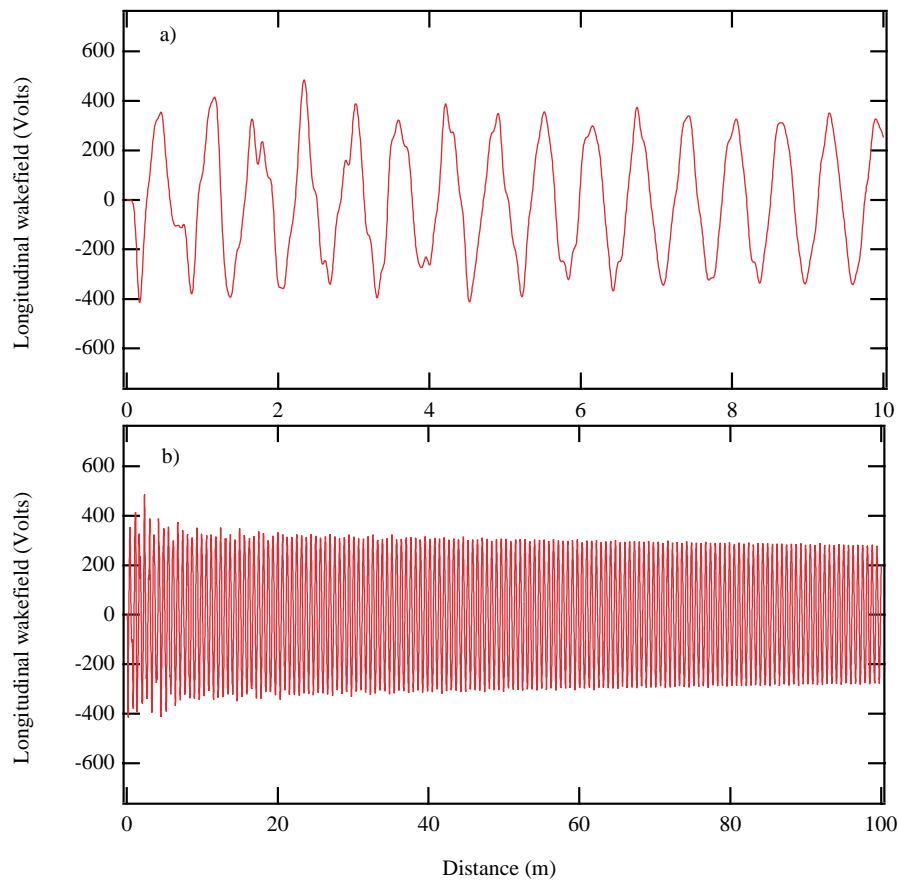

FIG. 3. (Color) Longitudinal wakefield calculated using MAFIA T3 with a 3 cm bunch length. (a) Short-range wake and (b) long-range wake.
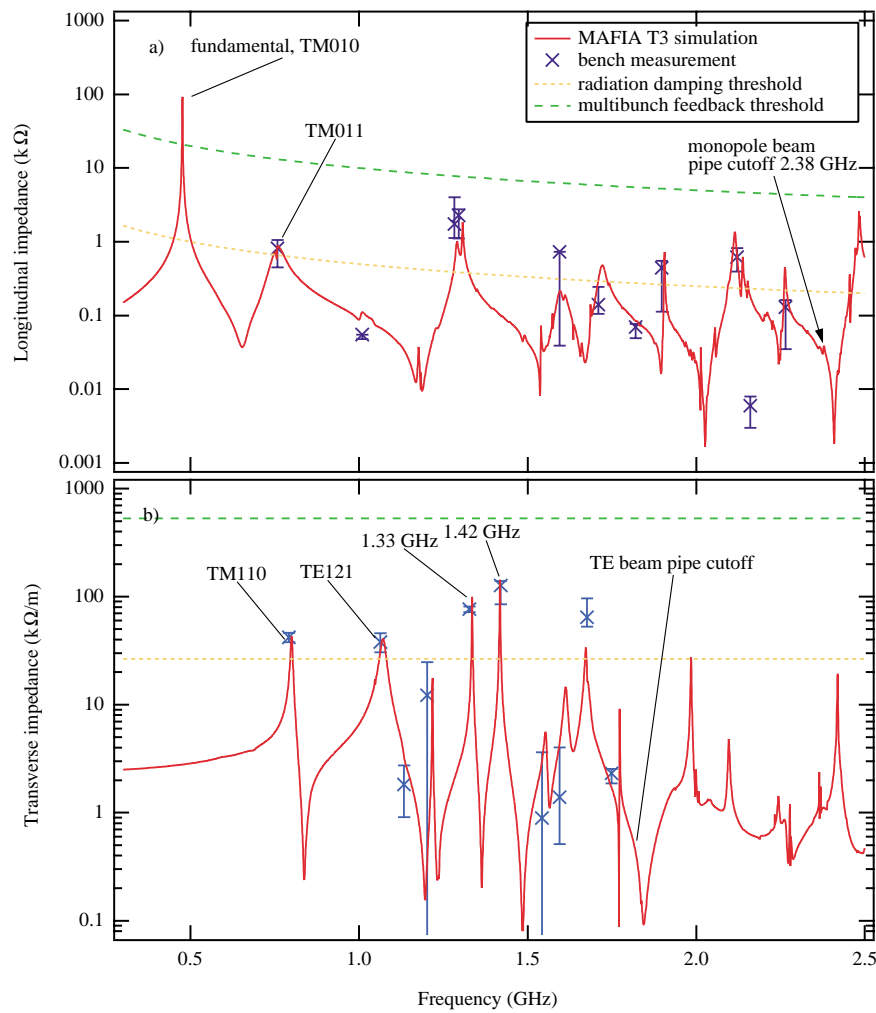
FIG. 4. (Color) Impedance spectra calculated from Fourier transforming time domain wakes and estimates of mode impedances measured in a cold-test model of the PEP-II cavity. The effective impedances for damping from synchrotron radiation and the multibunch feedback system at the nominal LER parameters are also shown. (a) Longitudinal impedance and (b) transverse impedance.

modes propagate. The threshold impedances for radiation damping and for the nominal damping rate of the longitudinal multibunch feedback system for the PEP-II low energy ring (LER) are also shown for reference. The wakes of all of the modes, except the fundamental mode, have fully decayed in the time domain and are fully resolved in the frequency domain. Because of the truncation in the time record of the wake, the fundamental mode is artificially broadened, giving it a lower impedance. Its impedance is better found using an alternate technique described later in this section.

The transverse impedance spectrum is shown in Fig. 4(b). The two dominant HOMs are marked as well as the TE cutoff frequency of the beam pipe. The residual beating observed in the time domain in Fig. 2(b) corresponds to the neighboring modes of 1.33 and 1.42 GHz. Also shown are the threshold impedances for radiation damping and for the nominal damping rate of the transverse multibunch feedback system for the PEP-II LER. The impedance of each HOM found in bench measure-

ments of a cold-test model is also shown along with an estimated error. These results are discussed in more detail in the next section.

Typical simulations run on this geometry used wakes of up to 400 m, which could be calculated overnight and resolve modes with peak widths as low as about 0.35 MHz, corresponding to loaded Q's from a few hundred at low frequency to several thousand at high frequency. The Q's can be found by fitting the individual peaks in the impedance spectrum, similar to the technique described in the next section to measure the Q's on the bench.

For higher Q modes, the mode strength can be determined by doing a separate simulation in which the mode is excited by a constant amplitude polarized point dipole source in the cavity rather than by a bunch, and the quasi-linear growth of the mode amplitude can be recorded, along with the field amplitude at certain times [12]. Once the mode pattern has been well established, the stored energy in the mode and time-averaged power flow out of the HOM ports can be computed. From this the damping of

the HOM can be found. This method has the advantage that the field distribution of the mode is recorded so that the shunt impedance and Q_0 can also be calculated but the disadvantage that it is tedious to iterate for many modes.

III. COMPARISON WITH BENCH MEASUREMENTS

Extensive low-power measurements were made on a cold-test model of the PEP-II cavity to verify the damping of the HOMs. Details of these measurements and techniques are given elsewhere [10]. This section summarizes the results and compares them with the simulated results from the previous section.

The impedance of each mode was found by independently measuring R/Q and Q and computing the product. On axis and off axis bead pulls were used to measure the R/Q of monopole and dipole modes, respectively. The bead pull, or Slater perturbation technique [13], uses the fact that a small perturbing object, usually a dielectric bead or metal needle, shifts the resonant frequency of a mode in proportion to the square of the electric field at the object. By measuring and integrating the field strength along the bead-pull axis, the R/Q of a mode can be determined.

Experimentally, the mode is excited using weakly coupled probe antennas in the beam pipe while a bead is pulled through the cavity. The frequency shift of the mode can be measured directly using a swept-frequency network analyzer, or, equivalently, the mode can be excited at a single frequency near resonance and the phase shift due the mode frequency change can be measured. We use the phase shift technique for our measurements because it is more sensitive to small frequency shifts.

Uncertainties in the bead-pull measurements result if the mode has either a small R/Q or is in a part of the spectrum with several nearby modes. For example, Fig. 5(a) shows the bead pull for the 1327 MHz dipole mode (vertical orientation) 4 cm off axis. The measurement is clean and repeatable with little drift, giving confidence in the R/Q value. Figure 5(b) shows a bead-pull measurement for the 1595 MHz monopole mode. Clearly the signal is much weaker (less than 1° of phase perturbation), and there is considerable drift and noise. A linear interpolation is made between the starting and ending points of the integration in an attempt to account for slow drifts such as temperature variations, but this does not correct for nonlinear drifts, noise, or other disturbances. Repeated measurements of the same mode gave lower numbers for the R/Q so the error range was expanded accordingly. The calculated values at the peaks, the measured values, and estimates of errors are listed in Tables I and II.

The Q was found by measuring the transmission between weakly coupled probe antennas in the beam pipe and carefully fitting the response. The antennas were placed off the beam axis on azimuthally rotatable fixtures to help distinguish monopole and dipole modes by preferentially exciting these modes. This was usually helpful in identifying the mode along with bead-pull results. Measurements
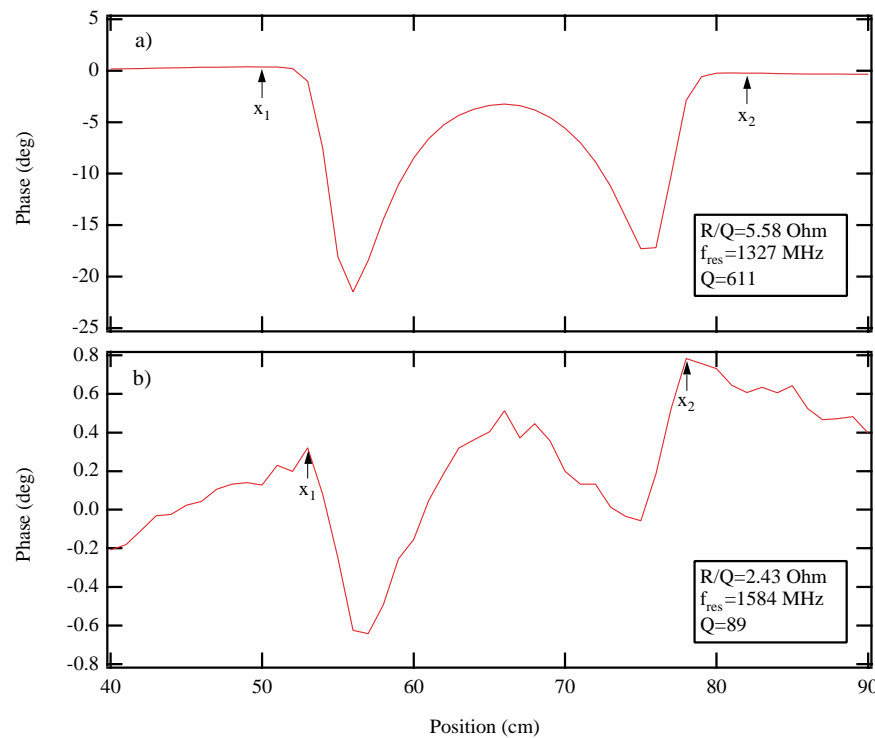

FIG. 5. (Color) Examples of bead-pull measurements. (a) The relatively strong 1327 MHz dipole mode shows an easily measurable phase shift. (b) 1595 MHz monopole mode provides a small phase shift with appreciable drift during the measurement.

TABLE I.   Impedance and Q's of monopole modes estimated from calculations and measurements. $R = V^2/2P$. n.m. = not measured, n.v. = not visible, n.r. = not resolved in time domain simulation.

$f_{r,\mathrm{meas}}$ (MHz)	R/Q_{meas} (Ω)	Q_{meas}	R_{meas} (Ω)	$f_{r,\mathrm{calc}}$ (MHz)	R_{calc} (Ω)	Q_{calc}
476	$117.3^{+0.00}_{-18.5}$	32 469	3.809×10^6	476	n.r.	
758	44.6 ± 13.4	18^{+0}_{-4}	809^{+241}_{-362}	758	879	15
1009	$0.43^{+0.00}_{-0.048}$	128^{+0}_{-3}	55^{+0}_{-7}	1010	35	100
1283	$6.70^{+6.4}_{-0.00}$	259^{+47}_{-92}	1736^{+2272}_{-617}	1291	1013	88
1295	10.3 ± 2.1	222^{+0}_{-88}	2287^{+455}_{-1184}	1307	1831	203
1595	$2.43^{+0.00}_{-2.14}$	300^{+0}_{-170}	729^{+0}_{-691}	1596	214	52
1710	0.44 ± 0.11	320^{+125}_{-0}	141^{+104}_{-35}	1721	476	54
1820	0.13 ± 0.013	543^{+0}_{-120}	70^{+7}_{-21}	n.v.	n.v.	n.v.
1898	0.17 ± 0.043	2588^{+0}_{-1693}	442^{+111}_{-328}	1906	715	685
2121	1.82 ± 0.18	338^{+69}_{-100}	616^{+199}_{-226}	2113	1346	163
2160	0.053 ± 0.011	119^{+10}_{-35}	6^{+2}_{-3}	2153	293	300
2265	0.064 ± 0.016	1975^{+0}_{-1314}	126^{+32}_{-95}	2263	450	306
2344	n.m.	693^{+0}_{-511}	n.m.	n.v.	n.v.	n.v.

were made with a model of the cavity coupler in place and were made only below the beam pipe cutoff frequency. Results listed for the fundamental mode are for the unloaded impedance, and the Q value was extracted from an average of the measured value from the 26 production cavities.

The measurement uncertainty using this technique can be particularly large if the modes are strongly damped or are in a crowded part of the spectrum. In many cases the R/Q or Q are so low that the signals are barely visible or in some cases not visible at all. In cases where the modes are in a crowded part of the spectrum an attempt is made to identify the peaks by adjusting the antennas in the beam pipe to confirm the azimuthal character (monopole, dipole, or higher) of the modes while their longitudinal symmetry may be inferred from the bead pulls. In cases where the peaks are quite clear and strong signals can be measured for the Q and for the bead pull there is good agreement

between the calculated and measured values such as TM$_{011}$ at 758 MHz, TM$_{110}$ at 792 MHz, and TE$_{121}$ at 1133 MHz.

For example, Fig. 6(a) shows the spectrum in the region of the 1327 MHz dipole mode for several azimuthal orientations of the antennas. The spectra are quite clear and the two orientations of the dipole mode can be clearly separated and their Q's accurately measured. Figure 6(b) shows the crowded spectrum around the 1676 MHz dipole mode. Clearly there are other peaks present in the spectrum and an attempt is made to identify the most likely candidates for the vertical and horizontal components of the dipole. In case of uncertainty the range of possible fit values for Q is included in the error estimate.

As shown in Fig. 4, the calculated spectrum shows general agreement with the bench measurements, especially when taking the measurement uncertainty into account. In many cases the calculated impedance falls within the broad

TABLE II.   Transverse impedance and Q's of dipole modes estimated from calculations and measurements. $R_\perp = [R/(Qkr^2)]Q_L$. The measured R/Q is at a 4 cm offset. n.m. = not measured, n.v. = not visible.

| $f_{r,\mathrm{meas}}$ (MHz)	R/Q_{meas} (Ω)	Q_{meas}	$R_{\perp,\mathrm{meas}}$ (kΩ/m)	$f_{r,\mathrm{calc}}$ (MHz)	$R_{\perp,\mathrm{calc}}$ (kΩ/m)	Q_{calc}
792	9.69 ± 0.997	115	42.0 ± 4.2	800	38.7	96
1063	50.4 ± 10.1	27	38.0 ± 7.6	1071	40.1	34
1133	1.29 ± 0.65	54	1.82 ± 0.91	n.v.	n.v.	n.v.
1202	0.56 ± 0.56	871^{+13}_{-51}	$12.2^{+12.6}_{-12.2}$	1218	17.6	642
1327	5.58 ± 0.28	611^{+6}_{-7}	$76.7^{+4.6}_{-4.7}$	1335	99.5	510
1420	5.31 ± 0.53	1138^{+0}_{-289}	$126.9^{+12.6}_{-41.7}$	1417	143.7	554
1542	0.50 ± 0.50	92^{+94}_{-16}	$0.89^{+2.7}_{-0.89}$	1553	2.0	130
1595	0.51 ± 0.21	145^{+155}_{-56}	$1.39^{+2.6}_{-0.88}$	1611	11.6	180
1676	4.63 ± 0.46	783^{+285}_{-72}	$64.5^{+32.3}_{-11.8}$	1672	33.9	265
1749	0.10 ± 0.01	1317^{+0}_{-139}	$2.31^{+0.23}_{-0.45}$	1774	9.15	1234
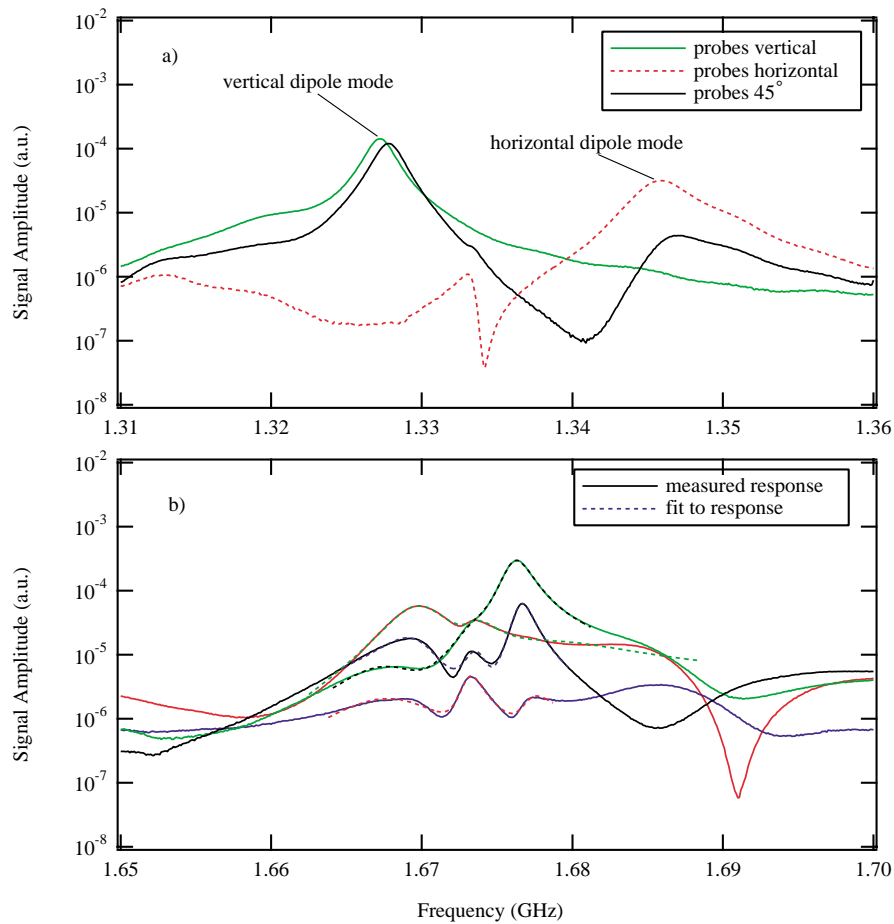
FIG. 6. (Color) Examples of measured transmission spectra on the bench at various probe angles. (a) For dipole modes which are well separated, determination of the Q is simple. (b) More crowded spectra require fitting to multiple peaks with different relative phases, resulting in a larger uncertainty.

range of uncertainty estimated by combining these errors. In a few cases the measured value is outside this range, possibly because the wrong peak was identified for the Q measurement or bead pull, the interpretation was overly conservative or not all sources of error were adequately accounted for. In cases where the uncertainty arises because the mode is inherently weak or is heavily damped, the mode is not significant because its impedance is well below the threshold for instability.

The numerical model has limitations in terms of the details of the geometry description, the total mesh size available and the length of wakefield that can be calculated in a reasonable time. The MAFIA model used here has a simplified coupler and does not show the low-frequency structure associated with standing waves between the cavity and the window which were seen in a cold-test model and the beam-based measurements. The minimum mesh size of 5 mm used for this model is adequate for approximating the main features of the cavity but could lead to inaccuracies in some of the mode frequencies because of the relatively coarse approximation of the nose cones. The length of the recorded wakefield (400 m) is adequate to resolve most of the peaks in the spectrum. The low Q modes

are adequately resolved with only a 100 m wake, but the impedance of some of these modes increases slightly when the wake length is increased to 400 m. Inspection of the wakes in Figs. 2 and 3 shows that there are no large components present at the end of the time record, other than the fundamental in Fig. 3. The HOM ports and other external coupling apertures are approximated by a broad band "open boundary" in MAFIA. In theory the HOM loads, like the coupling box, may have some reflections which could add structure to the real impedance spectrum. In practice the HOM loads are well matched over a very wide band, unlike the window which is inherently narrower band, and are unlikely to lead to significant errors below cutoff.

Table I summarizes the measured and calculated values for the monopole modes. Table II shows the same for the dipole modes, where both the measured and calculated impedances are for the orientation of the dipole modes which are not damped by the power coupler.

IV. BEAM-BASED HOM MEASUREMENTS

The PEP-II cavities are now in routine operation at SLAC at high current. Evidence from the longitudinal and
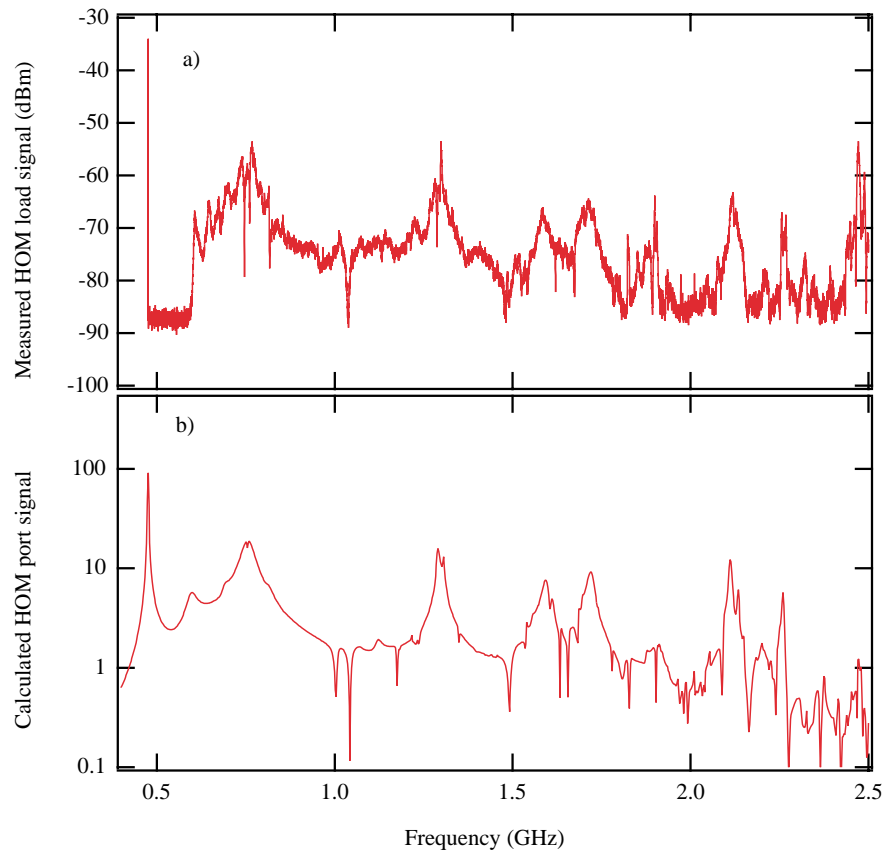
FIG. 7. (Color) Measured and calculated frequency spectrum of the signal reaching the HOM load. (a) Measured spectrum at rotation harmonics of a HOM port probe signal with a single bunch stored in the LER. The signal was uncalibrated. (b) Calculated spectrum of the signal at the HOM port from time domain simulation.

transverse feedback systems suggests that the actual mode strengths are consistent with expectations from cold-test model measurements [14,15]. During the commissioning of the storage rings we used a pickup antenna close to the load material to record the signals reaching one of the HOM loads. With a single bunch in the storage ring, the spectrum is a comb of lines at multiples of the rotation frequency of 136 kHz with varying amplitudes. We acquired the beam signals using a spectrum analyzer via a computer interface in small enough frequency bands such that individual rotation harmonics could be resolved. Figure 7(a) shows the amplitude of all of the rotation harmonics up to 2.5 GHz.

To simulate the signal reaching the HOM loads using MAFIA, a waveguide boundary condition is used at each port where the electromagnetic waves which satisfy the waveguide modes are allowed to propagate out without reflection. Figure 7(b) shows the Fourier transform of the calculated time domain signal reaching the port for frequencies up to 2.5 GHz.

There is good agreement between the simulation and measurement in the distribution, structure, and relative amplitudes of the peaks below the cutoff frequency. No attempt was made to compare the absolute signal amplitudes because the coupling of the signal probe to the HOM port

in the measurement was uncalibrated. The measured signal clearly shows the cutoff of the HOM waveguide at 600 MHz; the simulated port boundary in the MAFIA model is closer to the cavity and therefore shows more penetration by the frequencies below cutoff. While there is good general agreement between the spectra there is additional structure in the measured data, which was also visible in the measurements of the cold-test model. Some of this comes from coupling between the cavity modes and weak resonances in the coupling box, which is simplified in the MAFIA model by a broad band termination. In reality there are reflections from the window at frequencies other than the operating frequency and these cause weak resonances in the coupling box at HOM frequencies.

V. CONCLUSIONS

The PEP-II cavity is a successful design that is operating well and has made an important contribution to the rapid commissioning of PEP-II. We have presented a time domain simulation technique for calculating the residual impedance of highly damped structures which shows fairly good agreement for the strongest HOMs with bench measurements made on a cavity cold-test model. We believe the poor agreement of some of the weaker cavity HOMs

with the measurements is due to a combination of measurement uncertainties in determining the Q and the R/Q. Fortunately, these modes are generally too weak to be of concern. We can also use these techniques to calculate the beam spectrum observed at a HOM load, showing good qualitative agreement with beam observations. We believe these techniques can be applied successfully in future designs of damped rf structures for rapid optimization of the damping.

ACKNOWLEDGMENTS

————

[1] J. T. Seeman, in *Proceedings of the 1999 Particle Accelerator Conference, New York* (IEEE, Piscataway, NJ, 1999).

[2] S. Guiducci, in *Proceedings of the 1999 Particle Accelerator Conference, New York* (Ref. [1]).

[3] J. M. Byrd, K. Baptiste, S. De Santis, S. Kosta, C. C. Lo, D. Plate, R. A. Rimmer, and M. Franks, Nucl. Instrum. Methods Phys. Res., Sect. A **439**, 15–25 (1999).

[4] R. A. Rimmer and D. Li, in *Proceedings of the 1999 Particle Accelerator Conference, New York* (Ref. [1]).

[5] NLC Design Group, LBNL-PUB-5424, SLAC Report No. 474, UCRL-ID-124161, 1996.

[6] R. A. Rimmer *et al.,* LBNL Report No. LBNL-45136, SLAC Report No. LCC-0032, 1999.

[7] G. Conciauro and P. Arcioni, in Proceedings of the European Particle Accelerator Conference, Nice, 1990 (unpublished), pp. 149–151.

[8] N. Kroll and D. Yu, Part. Accel. **34**, 231–250 (1990).

[9] J. C. Slater, *Microwave Electronics* (Dover, New York, 1969).

[10] R. A. Rimmer *et al.,* in *Proceedings of the 1996 European Particle Accelerator Conference, Sitges, Spain* (PEP-II AP Note No. 96-06, SLAC Report No. PUB 7211, LBNL Report No. LBNL 38929).

[11] X. E. Lin, K. Ko, and C. K. Ng, in *Proceedings of the 1995 Particle Accelerator Conference, Dallas* (IEEE, Piscataway, NJ, 1995).

[12] D. Li, R. Rimmer, and S. Kosta, in *Proceedings of the 1998 Linear Accelerator Conference, Chicago* (IEEE, Piscataway, NJ, 1998); D. Li *et al.,* in *Proceedings of the 1999 Particle Accelerator Conference, New York* (Ref. [1]).

[13] L. C. Maier, Jr. and J. C. Slater, J. Appl. Phys. **23**, 68 (1952).

[14] M. Minty *et al.,* in *Proceedings of the e^+e^- Factories Workshop, Tsukuba, 1999,* edited by K. Akai and E. Kikutani (KEK, Tsukuba, 2000), pp. 160–166.

[15] S. Prabhakar, D. Teytelman, J. Fox, A. Young, P. Corredoura, and R. Tighe, in *Beam Instrumentation Workshop,* edited by R. O. Hettel, S. R. Smith, and J. D. Masek, AIP Conf. Proc. No. 451 (AIP, New York, 1998).